




# Tuning the Physical Properties of Ag and ZnO Nanoparticles to be Applied in Various Applications

ASMAA A.H. EL-BASSUONY <sup>1,4,5</sup> W.M. GAMAL,<sup>1</sup> ABEER F. IBRAHIM,<sup>2</sup> and H.K. ABDELSALAM<sup>3</sup>

1.—Physics Department, Faculty of Science, Cairo University, Giza 12613, Egypt. 2.—Department of Textile Printing Dyeing and Finishing, Higher Institute of Applied Arts 5th Settlement, New Cairo 11835, Egypt. 3.—Basic Science Department, Higher Institute of Applied Arts, 5th Settlement, New Cairo 11835, Egypt. 4.—e-mail: asmaa@sci.cu.edu.eg. 5.—e-mail: asmaa.ali@cu.edu.eg

Silver nanoparticles (Ag-NPs) accompanied by zincite (ZnO) and hematite ( $\text{Fe}_2\text{O}_3$ ) (Ag-Z-H) at different annealing temperatures (as dried, 400°C) were prepared using the Flash auto-combustion method. X-ray diffraction pattern assured the cubic structure of Ag-NPs for both samples. The morphology using atomic force microscopy assured the formation of nanoparticles with small agglomeration. By increasing the annealing temperature, the crystallite and particle sizes increased. Moreover, Fourier transforms infrared analysis assured the bond formation of the nanoparticles. The magnetic measurement indicated the increase of the coercivity ( $H_c$ ) of (Ag-Z-H) nanoparticles at 400°C by nine-fold compared with the as-dried sample. Contrarily, the as-dried (Ag-Z-H) nanoparticles showed 1.8-fold larger saturation magnetization ( $M_s$ ) than at 400°C. The high-frequency application was studied from the magnetic measurement and showed that both samples could be applied in the ultra-high frequency microwave region in the P band. As a result of the antimicrobial study, (Ag-Z-H) nanoparticles at 400°C showed stronger antimicrobial activities than the as-dried sample. Thus, the strong recommendation of as-dried (Ag-Z-H) nanoparticles at 400°C could be used as an effective alternative antibacterial drug, especially (Ag-Z-H) nanoparticles at 400°C.

## INTRODUCTION

Scientists from various fields have become interested in nanoparticles because of their unique physical and chemical properties. Silver nano-ferrite, -hematite, and -zinc oxide are all examples that have been the subject of substantial research because of their remarkable magnetic, electrical, and antibacterial properties.<sup>1,2</sup> Silver nanoparticles are small particles composed of silver, characterized by their nanoscale size, often falling within the 1–100-nanometer range. Due to the unique properties of silver nanoparticles, they are attracting considerable interest in several domains, such as textile printing, dyeing, and finishing. The combined inves-

tigation of silver and zinc nanoparticles has been performed because of their potential to generate effective antibacterial agents.

Furthermore, researchers are intensely interested in investigating the involvement of yeasts, bacteria, viruses, and molds in human pathology. An alarming increase in antibiotic resistance has prompted researchers to look for new antibacterial and antifungal nanomaterials.<sup>3–5</sup> Moreover, the many applications of nanomaterials have garnered significant interest from several researchers.<sup>6–8</sup> Silver nanoparticles (Ag-NPs) have been widely used as antiviral, anticancer, antibacterial, antifungal, and anti-inflammatory medicines.<sup>9,10</sup> Accordingly, an interesting and useful area of research for this topic is the antibacterial properties of Ag-NPs at different annealing temperatures. Physics, chemistry, and materials science researchers are interested in manufacturing Ag-NPs of different sizes

and shapes. Several methods are available for synthesizing silver nanoparticles (Ag-NPs), each generating different morphologies and thus offering many options for the material's possible uses. The current investigation used the flash auto-combustion technique to synthesize silver nanoparticles (Ag-NPs) characterized by their spherical morphology. Several nanoparticles with different magnetic characteristics and Ag-NPs have garnered much attention recently.<sup>11</sup> One of these nanoparticles (diamagnetic behavior) is zincite (ZnO), a naturally rare substance with a variety of industrial applications, particularly as a semiconductor crystal detector for dyeing and as antimicrobial nanomaterial.<sup>12</sup> Hematite ( $\text{Fe}_2\text{O}_3$ ) is a nanoparticle exhibiting ferromagnetic behavior. It is a naturally abundant material that has been extensively studied in previous studies because of its many industrial applications and ability to enhance physical properties.<sup>13</sup>

This research aims to investigate the influence of diamagnetic behavior (zincite) and ferromagnetic behavior (hematite) when combined with Ag-NPs at different annealing temperatures on their structural, magnetic, and antibacterial properties. A fascinating result in the magnetic measurement indicated the increase of the coercivity ( $H_c$ ) of (Ag-Z-H) nanoparticles at 400°C by nine-fold than the as-dried sample. Contrarily, the as-dried (Ag-Z-H) nanoparticles showed larger saturation magnetization ( $M_s$ ) by 1.8-fold than at 400°C. Therefore, the examined samples have useful applications, especially in biomedical areas such as magnetic targeting and separators.

## EXPERIMENTAL METHOD

### Synthesis of Nanoparticles

Figure 1 shows a flow chart of the preparation method of Ag-NPs accompanied by zincite and hematite nanoparticles at different annealing temperatures (as-dried—400°C) by the Flash auto-combustion method. The utilized raw materials were 1.5289 g silver nitrate ( $\text{AgNO}_3$ ), 0.5950 g zinc nitrate ( $\text{Zn}(\text{NO}_3)_2 \cdot 6\text{H}_2\text{O}$ ), 19.7960 g iron III nitrate ( $\text{Fe}(\text{NO}_3)_3 \cdot 9\text{H}_2\text{O}$ ), and 8.0120 g urea from Fisher Co. They were mixed with a small amount of distilled water with constant stirring for half an hour. After that, the mixture was put on a heater at 250°C till a fine powder was produced. The as-prepared sample was ground for half an hour; the other sample was then annealed at 400°C for 2 h. Finally, the resulting sample was ground for half an hour after annealing.

### Characterization

The x-ray diffraction pattern (XRD) was measured using the PANalytical XPert PRO device ( $\text{Cu-K}\alpha = 1.54 \text{ \AA}$ ). Fourier transforms infrared (FTIR) analysis was carried out on a Jasco FTIR 300 E spectrometer. FESEM was measured using an SEM

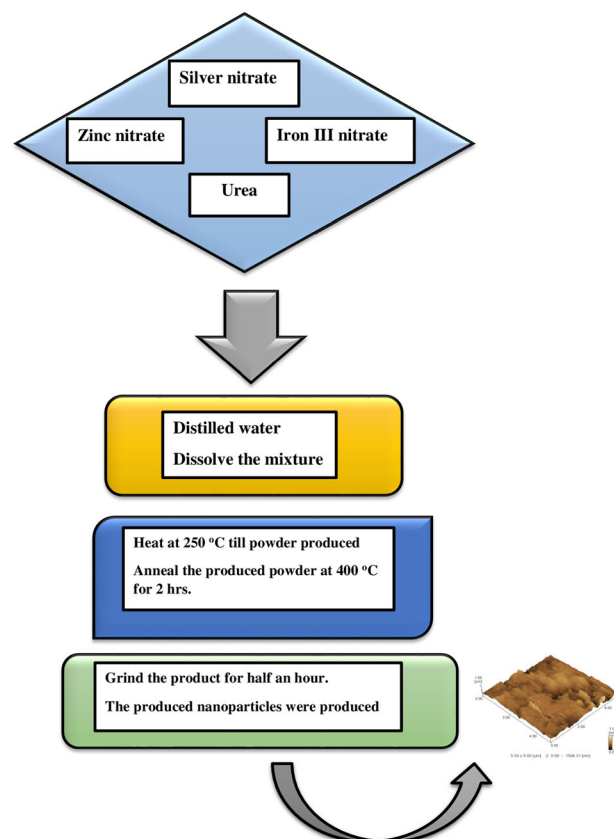


Fig. 1. Schematic diagram of as-dried (Ag-Z-H) nanoparticles at 400°C by Flash autocombustion method.

Model Quanta 250 FEG with an energy dispersion x-ray analysis (EDX) unit. Furthermore, atomic force microscopy was performed utilizing the Non-Contact Mode Wet—SPM-9600. Magnetic measurements were made using a Lake Shore 7410 vibrat sample magnetometer (VSM).

### Preparation of Antimicrobial Tests

Using a modified Kirby-Bauer disc diffusion technique,<sup>14</sup> nanometric (Ag-Z-H) at different annealing temperatures (as dried, 400°C) were evaluated in vitro against several Gram-positive, Gram-negative, and some fungal bacteria. After incubating the material of interest with the studied microorganisms at 30°C for 24–48 h, the widths of the inhibitory zones were recorded. Antimicrobial discs were compared to standards made of ampicillin (an antibacterial drug) and amphotericin B (an antifungal agent). Negative control was created using filter discs saturated with 10  $\mu\text{l}$  of solvent (deionized water, chloroform, DMSO).

## RESULTS AND DISCUSSION

### XRD Study

Figure 2 displays x-ray diffraction patterns (XRD) of as-dried Ag-NPs at 400°C accompanied by zincite (ZnO) and hematite ( $\text{Fe}_2\text{O}_3$ ) nanoparticles (Ag-Z-H).

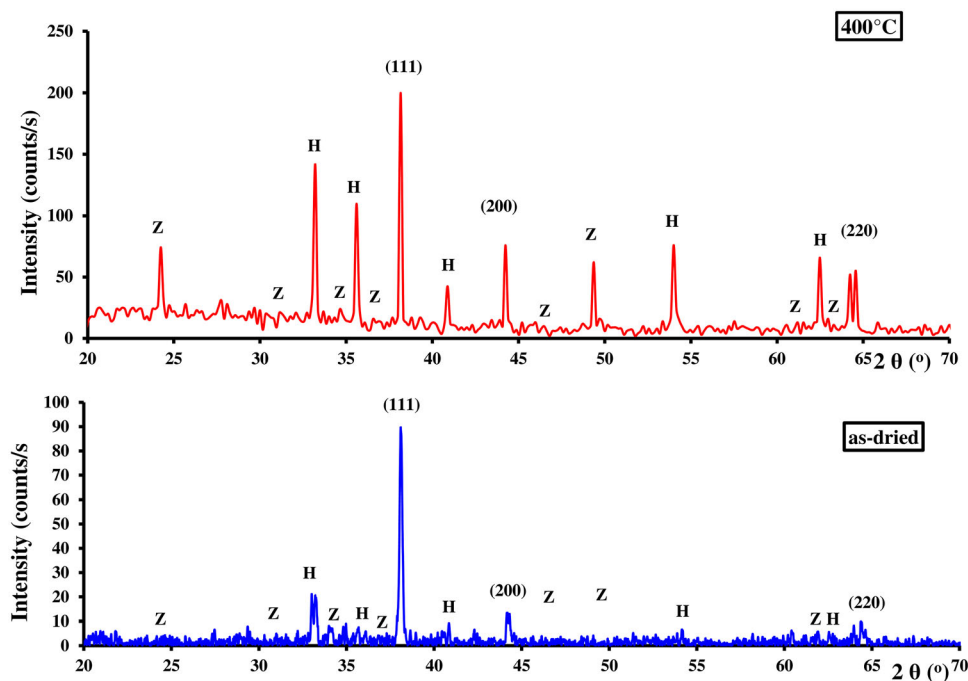


Fig. 2. XRD pattern of as-dried (Ag-Z-H) nanoparticles and at 400°C.

**Table I. Values of the crystallite size, particle size from FESEM, particle size from AFM, roughness, lattice parameter  $a$ , unit cell volume of as-dried (Ag-Z-H) nanoparticles, and at 400 °C**

Samples	Crystallite size (nm)	Particle size AFM (nm)	Roughness ( $\mu\text{m}$ )	$a$ ( $\text{\AA}$ )	$V$ ( $\text{\AA}^3$ )
As dried	14.6	106.8	2.02	4.092	68.5
400°C	26.5	116.93	1.8	4.081	67.9

The figure showed that by increasing the annealing temperature at 400°C the crystallinity increased, and the intensity of the peaks increased. This means that the effect of diamagnetic behavior increased at 400°C, which affected on the decrease of the magnetization as discussed below, because of the increase in the intensity of the peaks of Ag-NPs and zincite (ZnO). The diffraction peaks were indexed using ICDD cards of the cubic structure of Ag-NPs (04-004-6434), hexagonal structure of zincite (04-006-2073), and rhombohedral hematite (04-005-4425). The wideness of the peaks is an indication of the small crystallite size, and their values are reported in Table I. Moreover, the crystallite size increased by increasing the annealing temperature because of the increase of the crystallinity. The crystallite size was determined using Debye Scherrer's formula:<sup>15</sup>

$$D = \frac{k\lambda}{\beta \cos \theta} \quad (1)$$

where  $\lambda$  is the wavelength of Cu-K $\alpha$  = 1.54  $\text{\AA}$ , shape factor  $k$  = 0.9, and  $\beta$  is the full width at half maximum (FWHM) in radians. Table I displays the values of the crystallite sizes, lattice

parameters, and unit cell volume calculated based on the cubic structure of Ag-NPs. The lattice parameters with the cubic structure of Ag-NPs agreed with earlier reports.<sup>2,16</sup>

### FTIR Study

The results of the FT-IR (fourier transforms infrared) measurements on the samples under study are shown in Fig. 3 and Table II. In as-dried Ag-NPs and at 400°C, the bands 3432.7 and 3435.6  $\text{cm}^{-1}$  (peak 8) were allocated to the stretching vibration of the OH group, whereas bands 1630.5 and 1629.6  $\text{cm}^{-1}$  (peak 5) were allocated to the C=O vibration group. Other bands at 1376.9 and 1383.7  $\text{cm}^{-1}$  (peak 4) were attributed to C-N stretching vibration because of the metal nitrate utilized in their manufacture.<sup>16</sup> Moreover, the bands at 1117.5 and 1118.5  $\text{cm}^{-1}$  (peak 3) were ascribed due to C=C stretching vibrations. The band 2377.8  $\text{cm}^{-1}$  was also identified as the frequency of the C-O-C stretching vibration (peak 6). The bands 2931.3 and 2921.6 (peak 7) were used to identify the C-H vibration group. The bands 449.3 and 467.7  $\text{cm}^{-1}$  (peak 1) were used to identify the octahedral site in both samples, whereas the bands

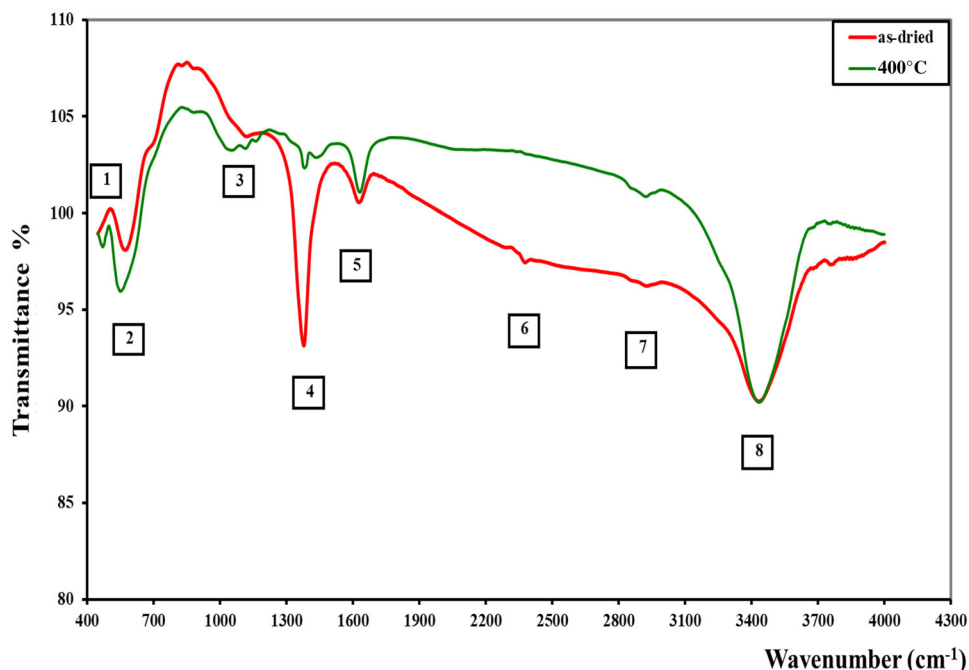


Fig. 3. FTIR spectra of as-dried (Ag-Z-H) nanoparticles at 400°C.

**Table II. Values of FTIR spectra of as-dried (Ag-Z-H) nanoparticles at 400°C**

No. of peaks	1	2	3	4	5	6	7	8
As dried	449.3	565.0	1117.5	1376.9	1630.52	2377.8	2931.3	3432.7
400°C	467.7	560.2	1118.5	1383.7	1629.6	—	2921.6	3435.6

565 and 560.2  $\text{cm}^{-1}$  (peak 2) were used to identify the tetrahedral site in the investigated samples. Results from FTIR were in accord with those from other studies.<sup>17,18</sup>

### AFM Study

Figure 4a is an atomic force microscopy (AFM) micrograph depicting the morphology of the examined nanomaterials. The morphology displays agglomeration owing to the lack of surfactant during preparation. The histogram of the average particle size and roughness of the studied nanomaterials, as derived from the AFM micrograph, is shown in Fig. 4b, and their respective values are listed in Table I. The (Ag-Z-H) nanoparticles at 400°C have a greater particle size than the as-dried (Ag-Z-H) nanoparticles. This was ascribed to increasing the annealing temperature, crystallite, and particle sizes. Moreover, the sample at 400°C showed excess Ag-NPs on the micrograph's surface, which act as a decoration of the diamagnetic Ag-NPs on the sample's surface. There is a correlation among the roughness, size, and surface activity of nanoparticles; the smaller the size of the nanoparticles, the higher the roughness and surface activity. Finally, the tested morphology using AFM

confirmed that the investigated samples were in the nano-size range.

### Magnetic Study

Figure 5a displays the M-H curve for as-dried (Ag-Z-H) nanoparticles at 400°C. Table III shows the computed values for the magnetic characteristics of the samples, including saturation magnetization ( $M_s$ ), coercivity ( $H_c$ ), residual magnetization ( $M_r$ ), squareness ( $R$ ), and magneto-crystalline anisotropy constant ( $k$ ).

The magneto-crystalline anisotropy constant ( $k$ ) was determined using the following formula<sup>19</sup>:

$$k = \frac{M_s H_c}{0.98} \quad (2)$$

The squareness was determined using the following Eq. 20:

$$R = \frac{M_r}{M_s} \quad (3)$$

The squareness value was used to identify the nature of the nanoparticle interactions. With a squareness value of  $< 0.5$  ( $R < 0.5$ ), the investigation samples assigned that the interaction between



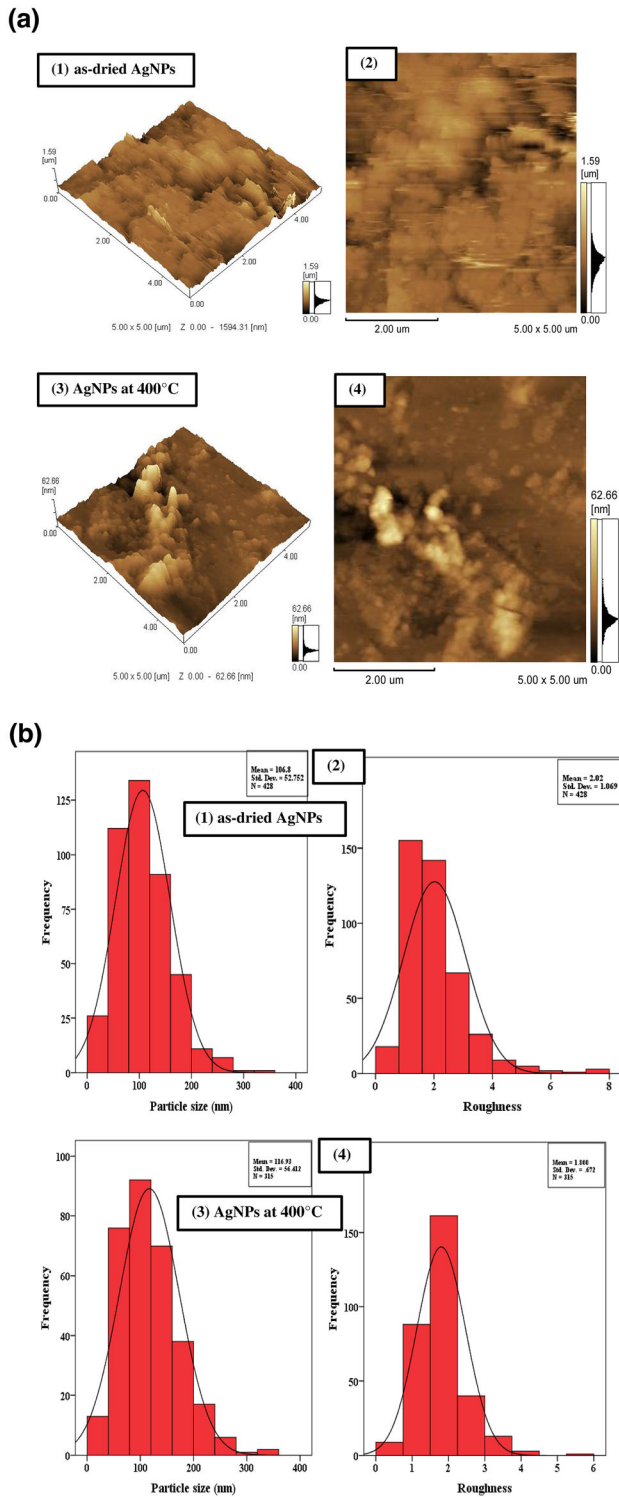


Fig. 4. (a) (1, 3) The 3D and (2, 4) plane image. (b) The histogram of the particle size and roughness of as-dried (Ag-Z-H) nanoparticles at 400°C.

nanoparticles for as-dried (Ag-Z-H) nanoparticles and at 400°C was magnetostatic. By raising the annealing temperature to 400°C, the saturation magnetization ( $M_s$ ) was reduced by 1.8-fold while

the coercivity ( $H_c$ ) rose by 9-fold compared to the as-dried (Ag-Z-H) nanoparticles. The decrease of  $M_s$  of (Ag-Z-H) nanoparticles at 400°C may be attributed to the increase in the crystallinity of the silver nanoparticles that agglomerate at the grain size. This agglomeration made a decoration of diamagnetic material on the sample's surface at 400°C as shown in the AFM micrograph, which decreased the  $M_s$ . Therefore, the influence of Ag-NPs and hematite on magnetism was the most significant, increasing the saturation magnetization of as-dried (Ag-Z-H) nanoparticles. In contrast to as-dried (Ag-Z-H) nanoparticles, the saturation magnetization  $M_s$  is lower in (Ag-Z-H) nanoparticles that have been annealed at 400°C because of the well-ordered crystal and the effect of two diamagnetic nanoparticles (silver and zincite). The increase in  $H_c$  of (Ag-Zn-H) at 400°C was 9-fold compared with that of as-dried because of the increase of the magneto-crystalline anisotropy constant ( $k$ ) by 5-fold and the decrease of the  $M_s$  by 1.8-fold of the sample at 400°C than that at as-dried according to Eq. 2.

Figure 5b displays the magnetic susceptibility ( $\chi = dM/dH$ ) field dependency of (Ag-Z-H) nanoparticles at different annealing temperatures. Consistent with the prior research, the magnetic susceptibility is greatest at zero fields. As seen in this figure, the increase in the distance between the two lines of the (Ag-Z-H) nanoparticles at 400°C was owing to the increase in coercivity ( $H_c$ ) compared to the as-dried (Ag-Z-H) nanoparticles. In addition, the saturation magnetization ( $M_s$ ) of as-dried Ag-NPs increased, resulting in a value of magnetic susceptibility that was 1.9-fold higher than that of (Ag-Z-H) nanoparticles at 400°C as shown in Table IV. As a result, the examined samples have useful applications, especially in biomedical ones such as magnetic targeting and separators.

### High-Frequency Application

Figure 6 and Table IV display the predicted operating frequency response of the examined samples based on magnetic measurements. The as-dried (Ag-Z-H) nanoparticles had a much higher operating frequency than (Ag-Z-H) nanoparticles annealed to 400°C. The nanomaterials' magnetism and devices' shape are only two aspects impacting the usable frequency ranges. The operating frequency of equipment may be used as a useful performance indicator. To determine the operating frequency ( $\omega$ ), the following relationship<sup>21-24</sup> was used.

$$\omega = 8\pi^2\gamma M \quad (4)$$

where  $M$  is the sample magnetization and  $\gamma = 2.8$  MHz/G is the gyromagnetic ratio. Consequently, the as-dried (Ag-Z-H) nanoparticles (846 MHz) and (Ag-Z-H) nanoparticles at 400°C (474 MHz) detected ultra-high frequency (UHF) in the microwave range of the P band.

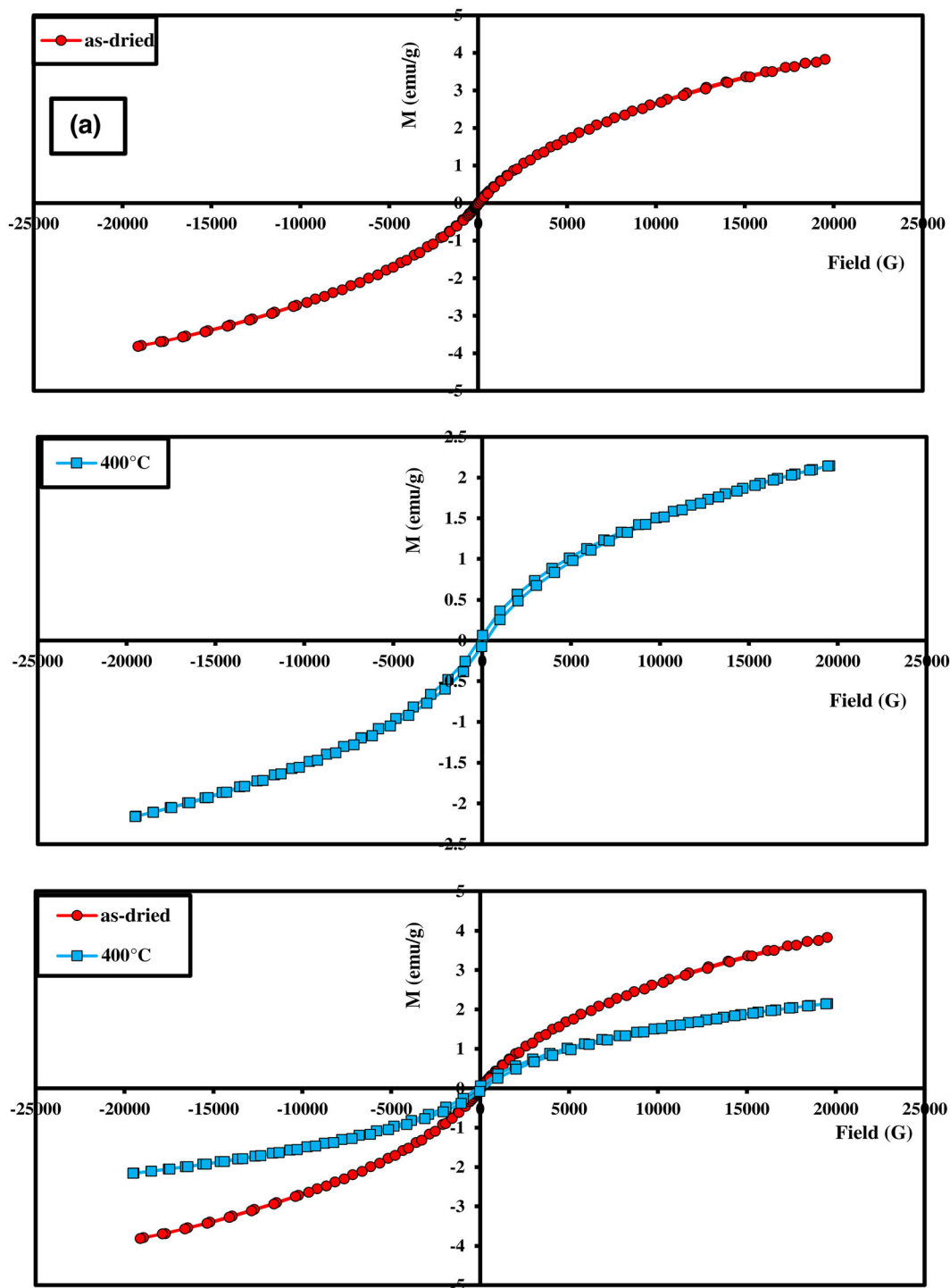


Fig. 5. (a) Magnetic measurements and (b) magnetic susceptibility of as-dried (Ag-Z-H) nanoparticles at 400°C.

### Antimicrobial Application

Figure 7a–c and Table IV illustrate the results of tests conducted on gram-positive, gram-negative, and fungal strains using (Ag-Z-H) nanoparticles both as-dried and at an annealing temperature 400°C. Both substances were ineffective against the tested fungus. However, the findings indicated that gram-positive bacteria such as *Bacillus subtilis*

(ATCC 6051), *Streptococcus faecalis* (ATCC 19433), and *Staphylococcus aureus* (ATCC 12600) and gram-negative bacteria like *Neisseria gonorrhoeae* (ATCC 19424), *Escherichia coli* (ATCC 11775), and *Pseudomonas aeruginosa* (ATCC 10145) offered remarkable treatment efficacy. The most efficient data are for the investigated sample at 400°C against gram-positive bacteria (*B. subtilis*, *S.*

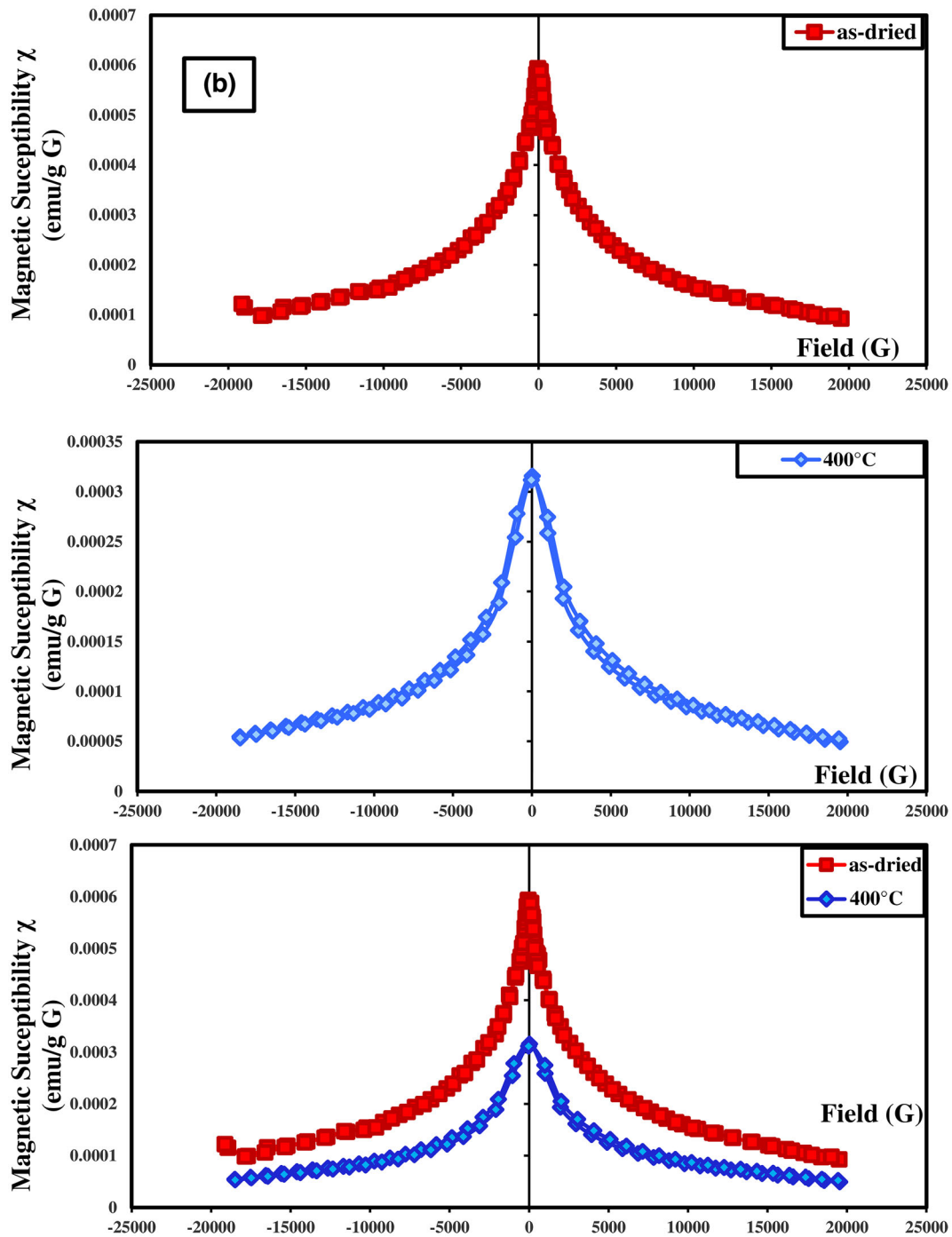


Fig. 5. continued

Table III. Magnetic parameters of as-dried (Ag-Z-H) nanoparticles at 400°C

Magnetic parameters	$H_c$ (G)	$M_s$ (emu/g)	$M_r$ (emu/g)	Squareness R	Magnetocrystalline anisotropy constant k (erg/g)	Magnetic susceptibility $\chi$ (emu/g G) $\times 10^{-4}$	$\Omega$ (GHz)
As dried	20.741	3.8209	0.0121	0.0032	80.87	5.94	0.846
400°C	187.20	2.1533	2.1456	0.0283	411.32	3.16	0.474

Table IV. The inhibition zone parameters of ampicillin, as-dried (Ag-Z-H) nanoparticles, and at 400°C

Samples	Inhibition zone diameter (mm/mg)									
	Bacteria					Fungi				
	G+					G-				
	<i>Bacillus subtilis</i>	<i>Staphylococcus aureus</i>	<i>Streptococcus faecalis</i>	<i>Escherichia coli</i>	<i>Neisseria gonorrhoeae</i>	<i>Pseudomonas aeruginosa</i>	<i>Aspergillus flavus</i>	<i>Candida albicans</i>		
As dried	12	15	13	13	13	13	0	0		
400°C	20	19	20	18	18	17	0	0		
Ampicillin	22	21	23	25	27	26	0	0		
Amphotericin B	0	0	0	0	0	0	16	19		

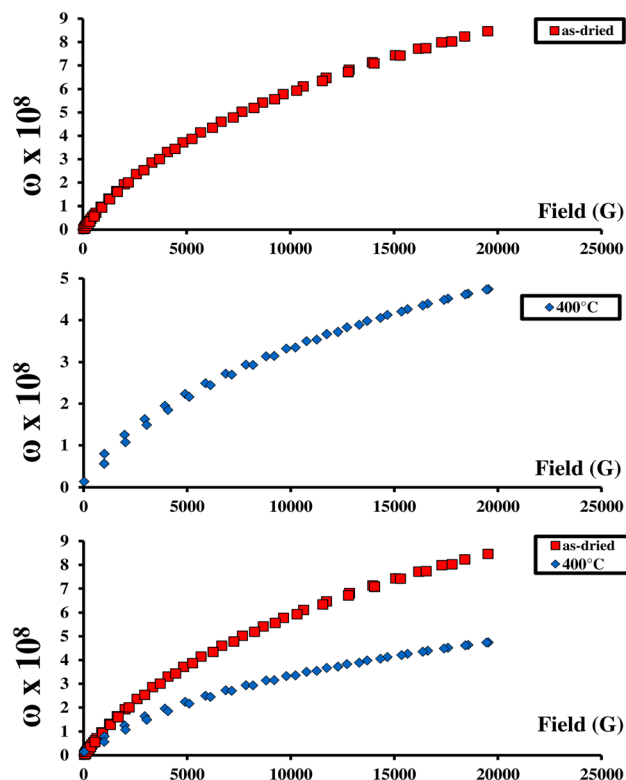


Fig. 6. Operating frequency of as-dried (Ag-Z-H) nanoparticles and at 400°C.

*faecalis*, and *S. aureus*) than that of the gram-negative bacteria. Furthermore, the treatment efficacy of (Ag-Z-H) nanoparticles at 400°C was greater on all tested strains than on as-dried (Ag-Z-H) nanoparticles. Due to the increase in crystallinity and intensity of the sample at 400°C according to XRD study, the combined toxicity of silver nanoparticles (Ag-NPs), zinc oxide (ZnO), and hematite (Fe<sub>2</sub>O<sub>3</sub>) is increased. Thus, the large effect of high-crystallinity nanoparticles against the studied bacteria led to an increase in toxicity for (Ag-Z-H) nanoparticles at 400°C compared to that of the as-dried sample. Therefore, the antibacterial activity of the Ag-NPs at 400°C is greater than that of the as-dried (Ag-Z-H) nanoparticles. A synergistic effect among Ag-NPs, zincite, and hematite had a strong ability to destroy the culture of the bacterial genetic material for as-dried samples. Moreover, the antibacterial properties increased for the sample at 400°C because Ag-NPs were being decorated at the surface of the sample as shown in the AFM micrograph, which increased the efficiency of Ag-NPs in destroying the bacterial cell. In addition, the Ag-NPs in both samples, with the zincite and hematite, effectively eliminated the bacterial DNA. It has been shown that the tested samples [(Ag-Z-H) nanoparticles at different annealing temperatures] impact the cell surface, which in turn destroys the bacterium's genetic material, killing it.<sup>25-40</sup> Therefore, both samples are highly suggested as alternate



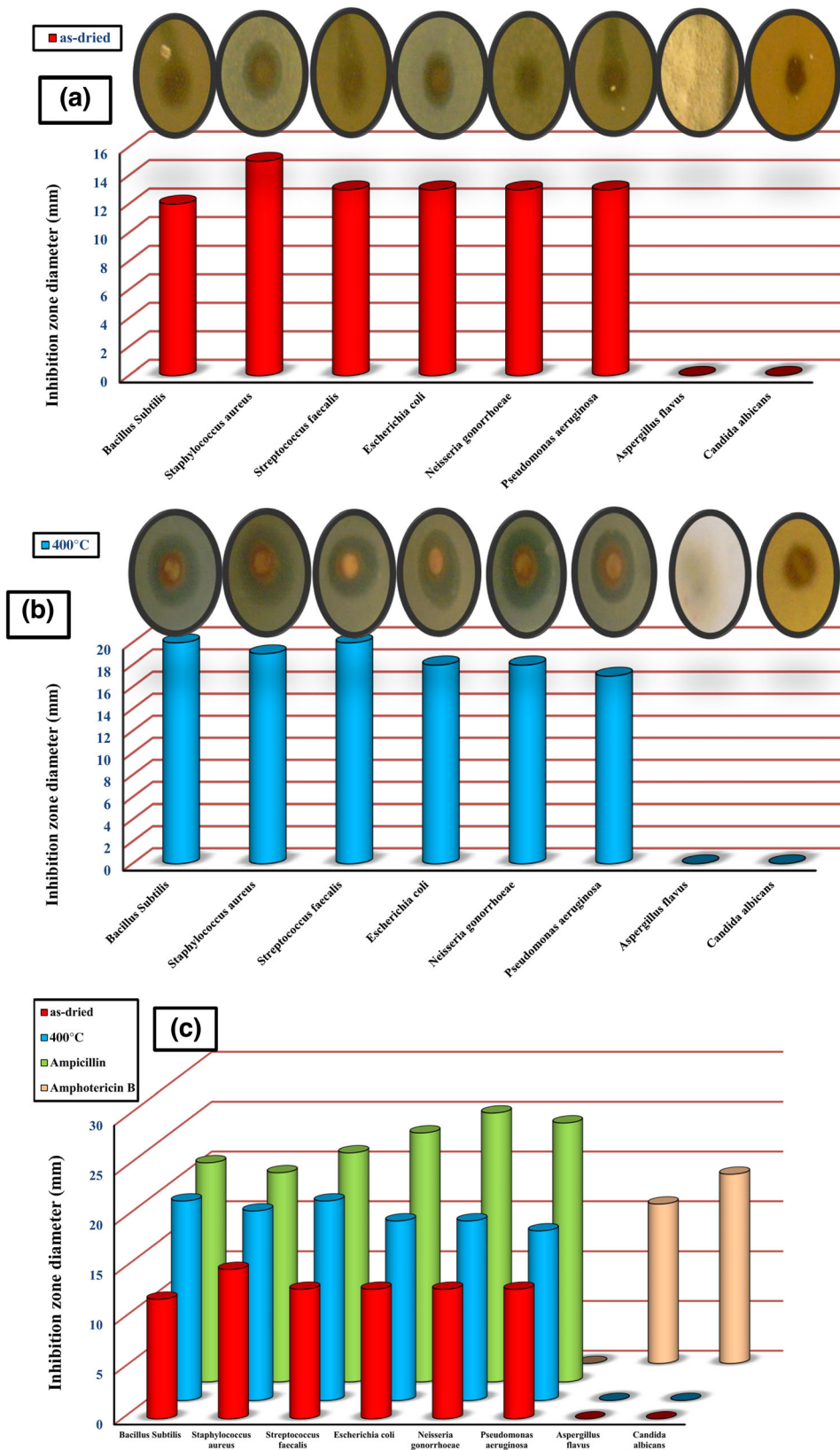


Fig 7. Antimicrobial diagram of (a) as-dried (Ag-Z-H) nanoparticles (b) at 400°C; (c) ampicillin, as-dried (Ag-Z-H) nanoparticles, and at 400 °C.

antibacterial nanomaterials, particularly (Ag-Z-H) nanoparticles at 400°C.

### CONCLUSION

The Flash auto-combustion method was used to synthesize silver nanoparticles (Ag-NPs) in combination with zincite (ZnO) and hematite (Fe<sub>2</sub>O<sub>3</sub>) (Ag-Z-H) nanoparticles at different annealing temperatures (as-dried—400°C). The x-ray diffraction (XRD) patterns of both samples confirmed the presence of a cubic structure in the Ag-NPs. Using atomic force microscopy (AFM) facilitated the morphological examination, which confirmed the production of nanoscale particles exhibiting agglomeration. As the annealing temperature increased, the crystallite and particle size increased. In addition, Fourier transform infrared (FTIR) analysis confirmed the bond formation of investigated samples. The magnetic measurement revealed that the coercivity ( $H_c$ ) of (Ag-Z-H) nanoparticles at 400°C increased nine times compared to the as-dried sample, which could be applied in sensors. On the other hand, the saturation magnetization ( $M_s$ ) of the nanoparticles (Ag-Z-H) in the as-dried sample exhibited a 1.8-fold increase compared to the nanoparticles heated at a temperature of 400°C, which could be used in magnetic targeting and separators. The high-frequency applications were determined by magnetic measurements, indicating that both samples are suitable for utilization within the ultra-high frequency (UHF) P-band microwave spectrum. The results of the antimicrobial investigation indicated that the antibacterial activity of (Ag-Z-H) nanoparticles was stronger when heated to a temperature of 400°C compared to the as-dried sample. Therefore, it is highly suggested that both samples of (Ag-Z-H) nanoparticles, especially those annealed at a temperature of 400°C, be considered a promising antibacterial therapy option.

### ACKNOWLEDGEMENTS

Not applicable.

### AUTHOR CONTRIBUTIONS

All authors contributed to data analysis, drafting, and revising the article. All authors read and approved the final manuscript.

### FUNDING

Open access funding provided by The Science, Technology & Innovation Funding Authority (STDF) in cooperation with The Egyptian Knowledge Bank (EKB). Not applicable.

### AVAILABILITY OF DATA AND MATERIALS

The data that support the findings of this study are available on request from the corresponding author.

### CONFLICT OF INTEREST

The authors declare no conflict of interest.

### CONSENT FOR PUBLICATION

Not applicable.

### ETHICS APPROVAL AND CONSENT TO PARTICIPATE

Not applicable.

### OPEN ACCESS

This article is licensed under a Creative Commons Attribution 4.0 International License, which permits use, sharing, adaptation, distribution and reproduction in any medium or format, as long as you give appropriate credit to the original author(s) and the source, provide a link to the Creative Commons licence, and indicate if changes were made. The images or other third party material in this article are included in the article's Creative Commons licence, unless indicated otherwise in a credit line to the material. If material is not included in the article's Creative Commons licence and your intended use is not permitted by statutory regulation or exceeds the permitted use, you will need to obtain permission directly from the copyright holder. To view a copy of this licence, visit <http://creativecommons.org/licenses/by/4.0/>.

### REFERENCES

1. H. Li, Q. Chen, J. Zhao, and K. Urmila, *Sci. Rep.* 5, 11033 (2015).
2. A.A.H. El-Bassuony, W.M. Gamal, and H.K. Abdelsalam, *J. Mater. Sci. Mater. Electron.* 33, 16219 <https://doi.org/10.1007/s10854-022-08516-y> (2022).
3. S. Honary, K. Ghajar, P. Khazaeli, and P. Schalchian, *Trop. J. Pharm. Res.* 10, 69 (2011).
4. W.M. Gamal, A.A.H. El-Bassuony, R.S. Hafez, and H.K. Abdelsalam, *JOM* 74, 4898 <https://doi.org/10.1007/s11837-022-05491-x> (2022).
5. M.F. Kuo, Y.H. Hung, J.Y. Huang, and C.C. Huang, *China Steel Tech. Rep.* 29, 44 (2016).
6. N.A. Kaskhedikar, and J. Maier, *Adv. Mater.* 21, 2664 (2009).
7. W.M. Gamal, A.A.H. El-Bassuony, and H.K. Abdelsalam, *Polym. Bull.* <https://doi.org/10.1007/s00289-023-04788-4> (2023).
8. C. Shan, Z. Ma, and M. Tong, *J. Hazard. Mater.* 268, 229 (2014).
9. A.A.H. El-Bassuony, and H.K. Abdelsalam, *Phys. Scr.* 98, 055919 <https://doi.org/10.1088/1402-4896/acc90c> (2023).
10. E.S. Anooj, S.J. Sreelekshmi, S.T. Gopukumar, and P.K. Praseetha, *Int. J. Pharm. Sci. Rev. Res.* 46, 22 (2017).
11. M.A. Sayed, A.A.H. El-Bassuony, and H.K. Abdelsalam, *Braz. J. Microbiol.* 51, 1475 <https://doi.org/10.1007/s42770-020-00366-2> (2020).
12. G. Lee, B. Lee, and K.T. Kim, *Environ. Sci. Nano* 8, 1690 (2021).
13. S.P. Schwaminger, R. Surya, S. Filser, A. Wimmer, F. Weigl, P. Fraga-Garcia, and S. Berensmeier, *Sci. Rep.* 7, 12609 (2017).

14. A.W. Bauer, W.M. Kirby, C. Sherris, and M. Turck, *Am. J. Clin. Pathol.* 45, 493 (1966).
15. X. Ning, Z. Xiong, B. Yang, W. Lu, and S. Wu, *Catalysts* 10, 314 (2020).
16. A.A.H. El-Bassuony, *JOM* 72, 1154 <https://doi.org/10.1007/s11837-019-03784-2> (2020).
17. R.D. Waldron, Infrared spectra of ferrites. *Phys. Rev.* 99, 1727 (1955).
18. A.A.H. El-Bassuony, and H.K. Abdelsalam, *JOM* 71, 1866 <https://doi.org/10.1007/s11837-019-03415-w> (2019).
19. B.B. Straumal, S.G. Protasova, A.A. Mazilkin, E. Goering, B. Baretzky, and P.B. Straumal, *Jetp Lett.* 97, 367 (2013).
20. M.S. Haque, M.F. Rahman, M.M. Zaman, M.A. Matin, A.K.M.A. Hakim, and M.F. Islam, *Appl. Mech. Mater.* 860, 87 (2016).
21. P. Akhtar, M.N. Akhtar, M.A. Baqir, A. Ahmad, M.U. Khallidoon, M. Farhan, and M. Azhar Khan, *J. Mater. Sci. Mater. Electron.* 32, 7692 (2021).
22. W.M. Gamal, A.A.H. El-Bassuony, H.K. Abdelsalam, and S.M. Abd El Wahab, *J. Mater. Sci. Mater. Electron.* 32, 21590 <https://doi.org/10.1007/s10854-021-06667-y> (2021).
23. M.N. Akhtar, M. Saleem, and M.A. Khan, *J. Phys. Chem. Solids* 123, 260 (2018).
24. A.A.H. El-Bassuony, H.K. Abdelsalam, and W.M. Gamal, *JOM* 74, 2656 <https://doi.org/10.1007/s11837-022-05170-x> (2022).
25. C.C. Berry, S. Wells, S. Charles, and A.S. Curtis, *Biomaterials* 24, 4551 (2003).
26. A.A.H. El-Bassuony, W.M. Gamal, and H.K. Abdelsalam, *Eur. Phys. J. Spec. Top.* 232, 1339 <https://doi.org/10.1140/epjs/s11734-022-00759-4> (2023).
27. H.N. Abdelhamid, A. Talib, and H.F. Wu, *RSC Adv.* 5, 34594 (2015).
28. A.A.H. El-Bassuony, W.M. Gamal, and H.K. Abdelsalam, *JOM* 74, 2635 <https://doi.org/10.1007/s11837-022-05315-y> (2022).
29. A.A.H. El-Bassuony and H.K. Abdelsalam, *Eur. Phys. J. Plus* 135, 66 <https://doi.org/10.1140/epjp/s13360-019-00025-y> (2020).
30. S.H. Kim, H.S. Lee, D.S. Ryu, S.J. Choi, and D.S. Lee, *J. Microbiol. Biotechnol.* 39, 77 (2011).
31. A. Maleki, H. Movahed, P. Ravaghi, and T. Kari, *RSC Adv.* 6, 98777 (2016).
32. R. Eivazzadeh-Keihan, F. Radinekiyan, H. Madanchi, H.A.M. Aliabadi, and A. Maleki, *Carbohydr. Polym.* 248, 116802 (2020).
33. A. Shaabani and A. Maleki, *Chem. Pharm. Bull.* 56, 79 (2008).
34. R. Eivazzadeh-Keihan, et al., *Chem. Eng. J.* 442, 136183 (2022).
35. A. Maleki, Z. Varzi, and F. Hassanzadeh-Afruzi, *Polyhedron* 171, 193 (2019).
36. Z. Hajizadeh, K. Valadi, R. Taheri-Ledari, and A. Maleki, *ChemistrySelect* 5, 2441 (2020).
37. V. Soltaninejad, M.R. Ahghari, R. Taheri-Ledari, and A. Maleki, *Langmuir* 37, 4700 (2021).
38. J. Rahimi, R. Taheri-Ledari, M. Niksefat, and A. Maleki, *Catal. Commun.* 134, 105850 (2020).
39. V. Soltaninejad and A. Maleki, *J. Photochem. Photobiol. A* 404, 112906 (2020).
40. Z. Varzi and A. Maleki, *Appl. Organometal. Chem.* 33, e5008 (2019).

**Publisher's Note** Springer Nature remains neutral with regard to jurisdictional claims in published maps and institutional affiliations.